

GT2011-46809

INVESTIGATION OF COOLING EFFECTIVENESS OF GAS TURBINE INLET FOGGING LOCATION RELATIVE TO THE SILENCER

Jobaidur R. Khan and Ting Wang
 Energy Conversion & Conservation Center
 University of New Orleans, New Orleans, LA 70148-2220, USA
 Email: jrkhan@uno.edu, twang@uno.edu

Mustapha Chaker
 BECHTEL Corporation, Houston, TX 77056, USA
 Email: mchaker@bechtel.com

ABSTRACT

The output and efficiency of gas turbines are reduced significantly during the summer, especially in areas where the daytime temperature reaches as high as 50°C. Gas turbine inlet fogging and overspray has been considered a simple and cost-effective method to increase the power output. One of the most important issues related to inlet fogging is to determine the most effective location of the fogging device by determining (a) how many water droplets actually evaporate effectively to cool down the inlet air instead of colliding on the wall or coalescing and draining out (i.e. fogging efficiency), and (b) quantifying the amount of non-evaporated droplets that may reach the compressor bellmouth to ascertain the erosion risk for compressor airfoils if wet compression is to be avoided. When the silencer is installed, there is an additional consideration for placing the fogging device upstream or downstream of the silencer baffles. Placing arbitrarily the device upstream of the silencer can cause the silencer to intercept water droplets on the silencer baffles and lose cooling effectiveness. This paper employs computational fluid dynamics (CFD) to investigate the water droplet transport and cooling effectiveness with different spray locations such as before and after the silencer baffles. Analysis on the droplet history (trajectory and size) is employed to interpret the mechanism of droplet dynamics under influence of acceleration, diffusion, and body forces when the flow passes through the baffles and duct bent. The results show that, for the configuration of the investigated duct, installing the fogging system upstream of the silencer is about 3 percentage points better in evaporation effectiveness than placing it downstream of the silencer, irrespective of whether the silencer consists of a single row of baffles or two rows of staggered baffles. The evaporation effectiveness of the staggered silencer is about 0.8 percentage points higher than the single silencer. The pressure drop of the staggered silencer is 6.5% higher than the single silencer.

NOMENCLATURE

C Concentration (kg/m³)

C_t Particle stochastic tracking time constant
 c_p Specific heat (J/kg-K)
 D Mass diffusion coefficient (m²/s)
 DA Dry air
 DBT Dry bulb temperature (K, °C, °F)
 d Droplet diameter (m)
 DPM Discrete phase model
 F Force (N)
 g Gravitational acceleration (9.81 m/s²)
 k Turbulence kinetic energy (m²/s²)
 k_c Mass transfer coefficient (m/s)
 h Convective heat transfer coefficient (W/m²-K)
 h_{fg} Latent heat (J/kg)
 m Mass (kg)
 Nu Nusselt number, hd/λ
 P Static pressure (N/m²)
 Pr Prandtl number, ν/α
 Re Reynolds number, ud/ν
 Sc Schmidt number (ν/D)
 Sh Sherwood number ($k_c d/D$)
 T Temperature (K, °C, °F)
 t Time (s)
 u Streamwise velocity component (m/s)
 u', T', C' Turbulence fluctuation terms
 v Spanwise velocity component (m/s)
 WBT Wet Bulb Temperature (K, °C, °F)
 x, y, z Coordinates (m)

Greek Letters

α Thermal diffusivity (m²/s)
 ω Specific dissipation rate (1/s)
 ε Turbulence dissipation rate (m²/s³)
 λ Heat conductivity (W/m-K)
 μ Dynamic viscosity (kg/m-s)
 ν Kinematic viscosity (m²/s)
 ρ Density (kg/m³)
 τ Stress tensor (kg/m-s²)
 σ Surface tension (N/m)

Subscript

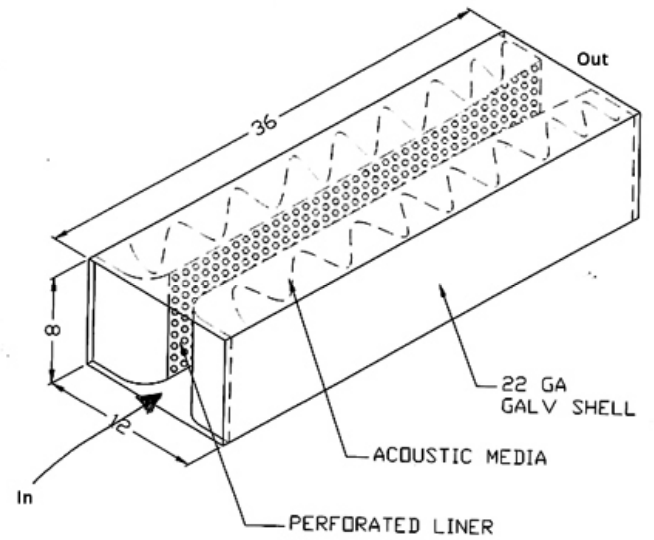
ex	Exit
i,j,k	Indices of direction
in	Inlet
p	Particle or droplet
t	Turbulent
x	x-direction (axial)
∞	Far away from droplets

INTRODUCTION

It is extremely important and required by law for a utility company to meet the peak-load demand during hot weather conditions. Land based gas turbines (GT) are often used to meet these demands. However, the power output and efficiency of gas turbines are reduced significantly during the summer because the air becomes lighter (which results in a lower mass flow rate), and the compressor's power consumption increases with increased ambient temperature.

It has been estimated that every 1°F rise of ambient air temperature reduces the gas turbine output by approximately 0.3 to 0.5% [1]. To increase the power output as well as the thermal efficiency, gas turbine inlet air-cooling is considered as the most convenient and cost-effective method. Among various cooling schemes, fog cooling (a direct evaporative cooling) has gained increasing popularity due to its simplicity and low installation cost at approximately \$40-60/kW. During fog cooling, demineralized water is atomized into micro-scale droplets inside the duct, where water particles have to go through a number of obstacles, e.g. the filter, the silencer, the trash screen, etc. The silencer is one of the most complicated obstacles in the duct. Angello [2] suggested periodic inspections of the silencers to monitor their conditions. Deterioration of the silencers can result in the ingestion of rust, metal fragments, and sound absorption material.

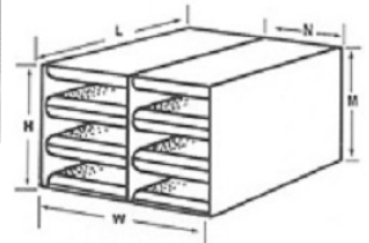
The silencer is used to reduce the noise before the bellmouth. There are a number of commercially available silencers with different shapes and sizes. Most of the silencers are used for HVAC (Heating, Ventilation, and Air Conditioning) purposes. Acoustical Surfaces, Inc. [3] manufactures silencers (Fig. 1a) for minimizing fan noise for air-conditioners. They are called "Silent-Mod Duct Silencers". The fan that moves air through modern HVAC systems is noisy, which could be annoying or intolerable in offices and rooms. While reducing objectionable fan noise, duct silencers can also reduce cross talk transmitted from one space to another through the ducts to insure office privacy. Silent-mod duct silencers are fabricated from 22-18 gauge galvanized steel for superior strength and maximum sound transmission reduction through the sidewalls. American Air Filter (AAF) [4] produces Rectangular Duct Mute (Fig. 1.b) to minimize stringent noise especially for gas turbine and compressor intake systems, and axial fans. UNCER Technologies Inc. [5] manufactures different types of silencers. They offer both horizontal (Fig. 1c) and vertical orientation of the baffles, which are made of G90 Galvanized steel. Industrial Acoustics Company (IAC) [6] is another manufacturer of HVAC duct silencers. They produce many different types of silencers for various purposes, e.g. for clean and hygienic air to hospitals, for reducing noise from building machine rooms etc. One silencer product produced by IAC is shown in Fig. 1(d).



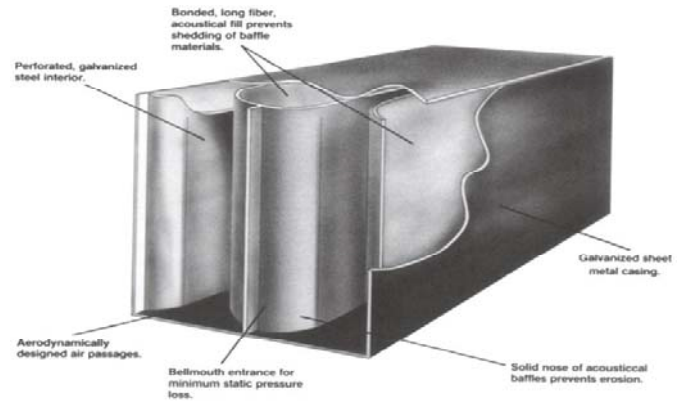
(a) Silent-Mod Duct Silencer



(b) Duct Mute Silencer



(c) UNCER Silencer



(d) IAC Silencer

Figure 1 Different types of silencers

The baffles of the silencer (as shown in Fig. 1) become obstacles for the air flow and collect water droplets if fogging is applied upstream of the silencer. Chaker et. al. [7-9] stated that a residence time of 1 to 2 seconds of unobstructed flow is ideal but rarely exists unless a special duct modification is made, or in a new gas turbine installation where extra duct sections can be incorporated at the design stage. Collisions of small water droplets with different parts in the ducts, including silencers, walls, and duct bends can lead to coalescence, forming thin liquid

layers on the surface or pooling of water on the duct floors. Under strong air stream shears, water filament formed on the wall opposite to the compressor bellmouth wetted by droplets recirculation, may be entrained by the high-speed flow and eventually enter the compressor.

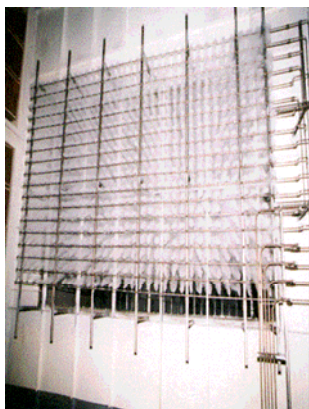


Figure 2. Fog Nozzle Manifold operating in the inlet duct of a GE-7EA gas turbine [7]

The configuration of gas turbine inlet ducts for most type of gas turbines allows sufficient residence time to most of the atomized water droplets to be evaporated before reaching the silencer. Consequently, nozzle manifolds for fogging application is generally installed upstream of the silencer. Wet compression type of cooling is typically installed downstream of the silencer. For some gas turbine, such as the actual LM2500 aeroderivative GT, the droplets residence time, if nozzle manifolds are installed upstream of the silencer, is relatively short. In this type of situation, the use of CFD help to determine which optimum location, upstream or downstream of the silencer, will provide the maximum evaporation efficiency. When the option of installing the nozzle manifolds downstream of the silencer is taken, the distance from the fogging system to the compressor bellmouth is shortened (so is the droplet residence time) and the chance that liquid water droplets may enter the compressor increases. To remedy the shortened droplet residence time to approach complete evaporation, additional duct sections can be installed, but the cost will increase. The trash screen is added with and without the fogging system in order to provide protection from object, which may flow through gas turbine inlet filter, and not the cooling system. The above discussion of the pros and cons of installing the fogging system either upstream or downstream of the silencer is a general description. The objective of this paper is to conduct a CFD simulation to provide quantitative information of fogging performance by studying the effects of the silencer's obstruction to pressure losses and water droplet evaporation processes including water droplet interaction with baffles and walls, droplet coalescence and breakup dynamics, and fogging efficiency. Two different silencers are taken into consideration, one having a single stage of baffles and another having two stages of staggered baffles. Their performances depend on (a) how many water droplets actually evaporate effectively to cool down the inlet air instead of colliding on the wall or coalescing and draining out (i.e. fogging efficiency), and (b) quantifying the amount of non-evaporated droplets that may reach the compressor bellmouth to ascertain the erosion

risk for compressor airfoils if wet compression is to be avoided.

NUMERICAL MODEL

Geometrical Configuration

The commercial software package FLUENT (version 6.2.16) from Ansys, Inc. is adopted for this study. Figure 3 shows different subdomains of a staggered silencer configuration in the 3D computational domain and post-processing planes. Several cross-sectional planes are selected in Fig. 3 to illustrate the computational results. Two different silencer geometries are used in this study. The length of the silencer sub-domain is 4.33m for the silencer with staggered baffles and 2.6m for the unit with a single row of baffles, as shown in Fig. 4. The duct configuration is taken from an existing LM2500 gas turbine system. Figure 5 shows the mesh for the side and top views and the magnified mesh over the baffles. Structured hexahedral meshes are used in the inlet sub-domain as seen in Fig. 5. The structured O-grid is used on the 2-D baffles and rest of the domain consists of unstructured meshes. The 2-D silencer subdomain is extruded in the z-direction to obtain the 3-D grid with uniform meshes throughout the longitudinal direction. Unstructured tetrahedral meshes are used in the duct domain to investigate grid sensitivity on the results. 121,000 and 231,000 meshes are used for comparison.

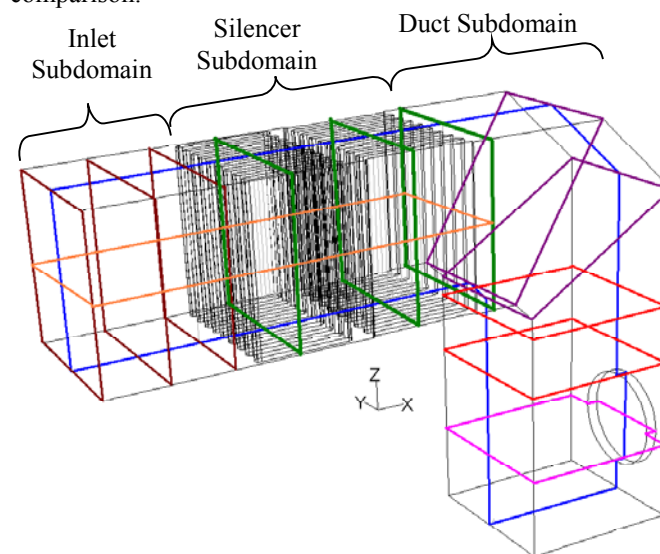


Figure 3 Gas turbine inlet duct showing different subdomains and post-processing planes

Governing Equations

The 3-D, time-averaged, periodically steady state Navier-Stokes equations as well as equations for mass, energy and species transport are solved. The transient governing equations are:

$$\frac{\partial \rho}{\partial t} + \frac{\partial}{\partial x_i} (\rho u_i) = S_m \quad (1)$$

$$\frac{\partial}{\partial t} (\rho u_j) + \frac{\partial}{\partial x_i} (\rho u_i u_j) = \rho \bar{g}_j - \frac{\partial P}{\partial x_j} + \frac{\partial}{\partial x_i} (\tau_{ij} - \rho \overline{u'_i u'_j}) + F_j \quad (2)$$

$$\frac{\partial}{\partial t} (\rho c_p T) + \frac{\partial}{\partial x_i} (\rho c_p u_i T) = \frac{\partial}{\partial x_i} \left(\lambda \frac{\partial T}{\partial x_i} - \rho c_p \overline{u'_i T'} \right) + \mu \Phi + S_h \quad (3)$$

where τ_{ij} is the symmetric stress tensor defined as

$$\tau_{ij} = \mu \left(\frac{\partial u_j}{\partial x_i} + \frac{\partial u_i}{\partial x_j} - \frac{2}{3} \delta_{ij} \frac{\partial u_k}{\partial x_k} \right) \quad (4)$$

The source terms (S_m , F_j and S_h) are used to include the contributions of water vapor mass, droplet forces, and evaporation energy from the dispersed phase (water droplets). $\mu\Phi$ is the viscous dissipation, and λ is the thermal conductivity in Eq. 3. The specific heat (c_p) in Eq. 3 is calculated from the mass-weighted value of specific heats of the gas and liquid components present in the domain. The effect of temperature on c_p values is negligible within the studied range between 30 and 50°C.

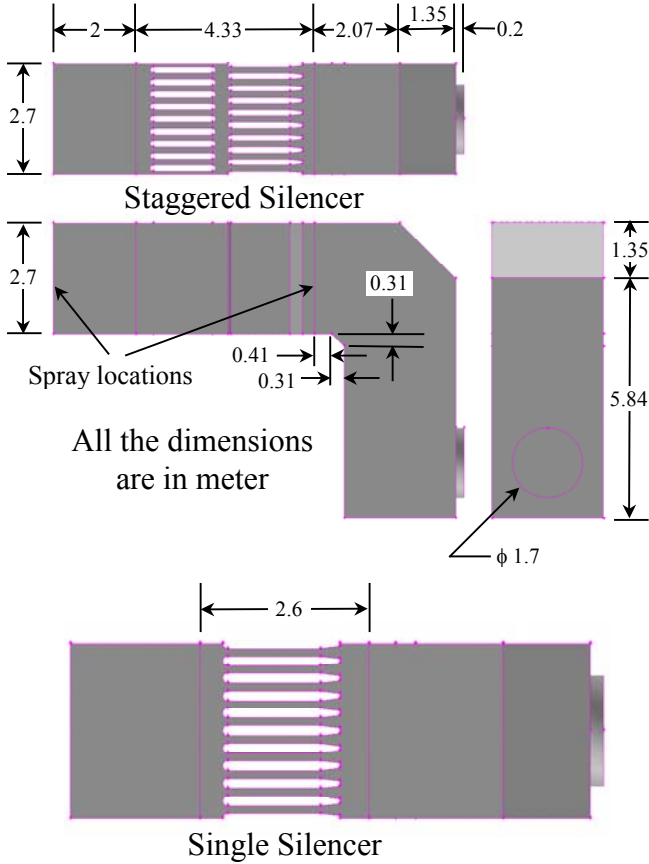


Figure 4 Dimension of the domain

During fog cooling, water droplets evaporate into vapor, which surrounds each droplet. The water vapor diffuses and is transported into the surrounding flow regime. The flow mixture consists of three main species: water vapor (H_2O), oxygen (O_2) and nitrogen (N_2). The equation for the species transport is:

$$\frac{\partial}{\partial x_i} (\rho u_i C_j) = \frac{\partial}{\partial x_i} \left(\rho D_j \frac{\partial C_j}{\partial x_i} - \rho \overline{u_i' C_j'} \right) + S_j \quad (5)$$

where C_j is the mass fraction of species j in the mixture, and S_j is the source term for this species. D_j is the diffusion coefficient.

Note that the terms $\rho \overline{u_i' u_j'}$, $\rho c_p \overline{u_i' T'}$, and $\rho \overline{u_i' C_j'}$ represent the Reynolds stresses, turbulent heat fluxes, and turbulent concentration (or mass) fluxes, which should be modeled properly for a turbulent flow.

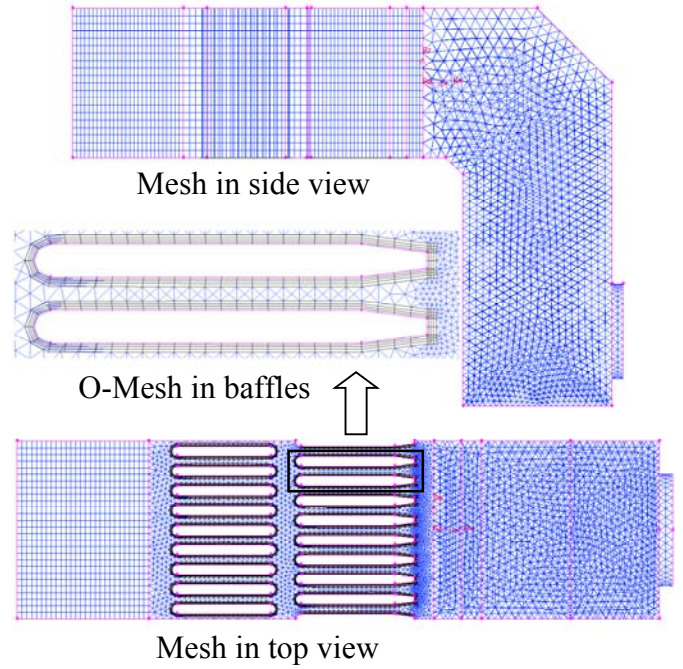


Figure 5 Meshed computational domain consisting of a mix of 231,000 structured and unstructured cells

Turbulence Models

As the duct encounters a high velocity airflow, the turbulence effect becomes significant. Considering the possible flow and droplets impinging on the baffles in the silencers and potential flow separations near the tailing edge of the baffles, the effects of turbulence models on the CFD calculation results need to be examined. Li and Wang [10] conducted a study focusing on examining the effects of five different turbulence models on mist/air film cooling effectiveness on turbine blades, which possesses some geometric similarities to the baffles. They tested the cooling by changing turbulence models, turbulence intensity, different forces acting upon the droplets, droplet sizes, particle tracking numbers, etc. They found the RSM (Reynolds Stress Model) and standard $k-\epsilon$ turbulence models produced consistent results. They also found that employing the stochastic tracking of droplets provided a notable change in the heat transfer and cooling effectiveness. Wang and Dhanasekaran [11] conducted a similar study on the effects of turbulence models on CFD results of mist/steam impinging jet cooling on a flat surface. Similar to the results of Li and Wang's mist film cooling [10], they reported that the RSM turbulence model provided the results most consistent with the experimental data and the standard $k-\epsilon$ turbulence model was proven robust with good results only next to the RSM model. In this present paper, a sensitivity study of using five different turbulence models is conducted and results (to be discussed later) are consistent with Dhanasekaran and Wang's finding. Since the $k-\epsilon$ turbulence model is robust and an order of magnitude faster than the RSM model, and there is no need to reach a more precise solution, the $k-\epsilon$ turbulence model with enhanced wall function is adopted in this study. The enhanced wall function is one of the several methods that model the near-wall flow. In the enhanced wall treatment, the two-layer model is combined with the wall functions.

The whole domain is separated into a viscosity-affected region and a fully turbulent region. A blending function is defined, which is equal to 0 in the viscosity-affected region and 1 in the fully turbulent region.

Dispersed-Phase Model (Water Droplets)

Droplet Flow and Heat Transfer – Based on Newton's 2nd Law, the droplets' motion in the airflow can be formulated by

$$\dot{m}_p d\mathbf{v}_p/dt = \sum \mathbf{F} = F_D + F_g + F_p + F_s \quad (6)$$

where m_p is the droplet mass, and v_p is the droplet velocity (vector). The right-hand side is the combined force acted on the droplets, which are F_D (drag force), F_g (gravity and buoyancy force), F_p (pressure force), F_s (Saffman lift force) etc. The following are the parameters of the various forces for the present study and their order of magnitudes. The density ρ_p and size d_p of particle are 998.2 kg/m³ and 10 μ m, respectively. The air density ρ_a is 1.23 kg/m³, and its dynamic viscosity coefficient μ is 1.85 $\times 10^{-5}$ kg/(m·s). Based on the CFD result, the average value of the pressure gradient $\partial p/\partial x$ is about 114 Pa/m. The maximum value of $(u_a - u_p)$ is near 10 m/s, where u_p and u_a the velocity of particle and air, respectively; the average value, $d(u_a - u_p)/dt$, is about 10 m/s². Finally, $f(Re_p) \sim 1.73$. Taking the above conditions into account, the magnitudes of the various forces can be acquired following Wang et. al.'s [12] study. The magnitude analysis shows that the drag force is the most important, followed by the Saffman force.

$$F_D = -3\pi d_p \mu (u_p - u_a) f(Re_p) \sim 4.6 \times 10^{-9} \quad (7)$$

$$F_g = \frac{1}{6} \pi d_p^3 (\rho_p - \rho_a) g \sim 5 \times 10^{-12} \quad (8)$$

$$F_p = -\frac{1}{6} \pi d_p^3 \frac{\partial P}{\partial x} \sim 2.6 \times 10^{-13} \quad (9)$$

$$F_s = 1.61 (\mu \rho_a)^{1/2} d_p^2 (u_a - u_p) \left| \frac{\partial u_a}{\partial y} \right|^{1/2} \sim 1.9 \times 10^{-9} \quad (10)$$

where, g is the gravitational acceleration, Re_p is the droplet Reynolds number and $f(Re_p)$ is the correction factor for the Stokes-drag force, which are expressed as follows:

$$Re_p = \frac{\rho_a |u_a - u_p| d_p}{\mu} \quad (11)$$

$$f(Re_p) = C_D Re_p / 24 \quad (12)$$

According to the Stokes law for $Re_p < 1$, $C_D Re_p / 24 = 1$. There are many models to formulate the term $C_D Re_p / 24$ for higher particle Reynolds numbers. Schiller and Naumann [13] correlated the expression up to $Re = 800$ as,

$$\frac{C_D Re_p}{24} = 1 + 0.15 Re_p^{0.687} \quad (13)$$

Without considering the radiation heat transfer, the droplet's heat transfer depends on convection, and evaporation is given as

$$m_p c_p \frac{dT}{dt} = \pi d^2 h (T_\infty - T) + \frac{dm_p}{dt} h_{fg} \quad (14)$$

where h_{fg} is the latent heat. The convective heat transfer coefficient (h) can be obtained with an empirical correlation [14-15]:

$$Nu_d = \frac{hd}{\lambda} = 2.0 + 0.6 Re_p^{0.5} Pr^{0.33} \quad (15)$$

where Nu is the Nusselt number, and Pr is the Prandtl number.

The mass change rate or vaporization rate in Eq. (14) is governed by the concentration difference between the droplet surface and the air stream:

$$-\frac{dm_p}{dt} = \pi d^2 k_c (C_s - C_\infty) \quad (16)$$

where k_c is the mass transfer coefficient, and C_s is the vapor concentration at the droplet surface, which is evaluated by assuming the flow over the surface is saturated. C_∞ is the vapor concentration of the bulk flow, and is obtained by solving the species transport equations. The values of k_c can be given from a correlation similar to Eq. (16) by [14-15].

$$Sh_p = \frac{k_c d}{D} = 2.0 + 0.6 Re_p^{0.5} Sc^{0.33} \quad (17)$$

where Sh is the Sherwood number, Sc is the Schmidt number (defined as ν/D), and D is the diffusion coefficient of the vapor in the bulk flow. When the droplet temperature reaches the boiling point, the following equation can be used to evaluate its evaporation rate [16]:

$$-\frac{dm_p}{dt} = \pi d^2 \left(\frac{\lambda}{d} \right) (2.0 + 0.46 Re_p^{0.5}) \ln(1 + c_p (T_\infty - T) / h_{fg}) / c_p \quad (18)$$

where λ is the gas/air heat conductivity, and c_p is the specific heat of the bulk flow.

Theoretically, evaporation can occur at two stages: (a) when the temperature is higher than the saturation temperature (based on local water vapor concentration), water evaporates, and the evaporation rate (Eq. 16) is controlled by the water vapor partial pressure until 100% relative humidity is achieved; (b) when the boiling temperature (determined by the air-water mixture pressure) is reached, water continues to evaporate at a rate that follows Eq. 18. After the droplet evaporates due to either high temperature or low moisture partial pressure, the water vapor is transported away from the droplet's surface due to convection and diffusion as described in the water vapor species transport equation (5).

Stochastic Particle Tracking - The turbulence effect on droplet dispersion cannot be simulated when the time averaged Navier-Stokes equation is solved because the particle tracks will follow the streamlines. A stochastic tracking method is adopted to overcome this issue. Basically, the droplet trajectories are calculated by using the instantaneous flow velocity ($\bar{u} + u'$) rather than the average velocity (\bar{u}). The velocity fluctuations are then given as:

$$u' = \zeta \left(\overline{u'^2} \right)^{0.5} = \zeta (2k/3)^{0.5} \quad (19)$$

where ζ is a normally distributed random number [16]. This velocity will apply during the characteristic lifetime of the eddy ($t_e = C_t (k/\epsilon)$), where C_t is a time constant to be specified according to the turbulent flow structure and the behavior of droplet dynamics. After this time period, the instantaneous velocity will be updated with a new ζ value until a full trajectory is obtained.

Boundary Conditions

Continuous Phase – In this study, the water is sprayed in such an amount, which is sufficient to saturate the inlet air. The inlet condition is set with an air speed at 10.51 m/s. This will give an air flow rate of 82.9 kg/s. The inlet

temperature is set at 50°C (323K) with 28% RH (Relative Humidity). The water vapor mass fraction at the inlet is set as the specific humidity of 0.0218 kg/kg dry air to ensure the desired RH. The inlet conditions of the turbulence are 1 m²/s² for the turbulence kinetic energy and 1 m²/s³ for the dissipation rate, which is equivalent to a turbulent intensity of 1%. The flow exit (outlet) is assumed to have a constant pressure. The temperature of the backflow (reverse flow), if any, is set at 50°C with 30% RH. The sidewall is non-slip (velocity is zero at the wall) and is assumed to be adiabatic.

The water at 305.2K (32.2°C) is atomized and injected at a velocity of 10 m/s. The calculated mass flow rate is 0.682 kg/s to reach saturation.

Dispersed Phase -- The droplet size is distributed in the range of 0.62 to 58.93 μm. Table 1 shows the droplet diameter distribution in terms of volume percentage. When the droplet reaches the wall, the droplet trajectory is determined from the discrete phase wall boundary condition. Each droplet when it approaches the wall can undergo one of several possible mechanisms based on the condition of the wall: dry or flooded.

In the case of **dry wall** (Fig. 6a), the droplets have three major regimes, including reflect, break-up, and trap. According to Watchers et al. [17], the regimes depend on the incoming Weber number of the droplet. Here, the Weber number is the ratio of kinetic energy of a droplet to the surface energy of a droplet ($We = \rho d u^2 / \sigma$). It was shown from the experimental results that droplets having Weber numbers less than 10 reflect elastically from the wall. When this value increases to more than 80, the droplet falls into the disintegration region, which leads to the droplet breaking-up into several smaller droplets. In the transition region ($30 < We < 80$), the droplet has a chance to either reflect or breakup. Apart from the above three facts, the droplets can be trapped by the superheated wall, and the entire mass will instantaneously pass into the vapor phase.

On the other hand, when the droplets impinge on a **flooded wall**, they have the chance for four different regimes, including splashing, spread, rebound, and sticking, as shown in Fig. 6b. Harlow and Shannon [18] obtained finite difference solutions to the Navier-Stokes equations for a viscous, incompressible liquid droplet impinging on a flat surface with and without liquid films. Bai and Gosman [19] developed a spray impingement model, which showed that the secondary droplets resulting from splashing had a certain distribution of sizes and velocities by analyzing the relevant impingement regimes and the associated post-impingement characteristics.

The wall film and reflect models are used in this study. The wall film model used in this study is based on the work of Stanton et al. [20] and O'Rourke et al. [21]. The four regimes stick, rebound, spread, and splash are based on the impact energy and wall temperature. Below the boiling temperature of the liquid, the impinging droplet can either stick, spread or splash, while above the boiling temperature, the particle can either rebound or splash. The impact energy is defined by

$$E^2 = (\rho V_r^2 d / \sigma) [1 / \{\min(h_0 / d, 1)\} + \delta_{bl} / d] \quad (20)$$

where V_r is the relative velocity of particle in the frame of the wall, h_0 is the length and δ_{bl} is the boundary layer thickness. The sticking regime is applied when the value of E becomes less than 16. Splashing occurs when the impingement energy is

above a critical E value of $E_{cr} = 57.7$. The splashing algorithm was followed as described in Stanton et al. [20].

At the outlet, the droplets just simply escape from the computational domain.

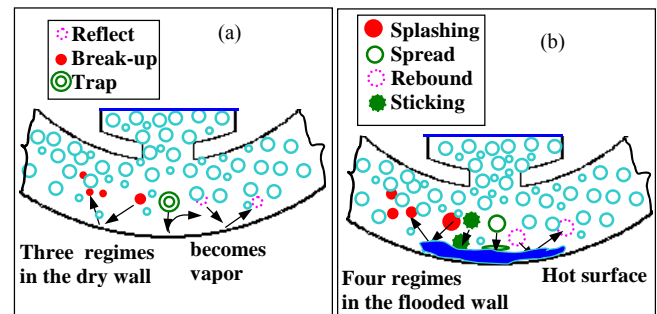


Figure 6 Droplet-wall interaction models [22]

Table 1 Water droplet diameter distribution

% Vol.	d (μm)	% Vol.	d (μm)
0.08	0.62	4.02	6.45
0.05	0.71	6.55	7.41
0.06	0.81	7.62	8.51
0.11	0.93	9.35	9.77
0.12	1.07	10.57	11.22
0.08	1.23	10.86	12.88
0.20	1.41	11.08	14.79
0.15	1.62	11.07	16.98
0.23	1.86	8.33	19.50
0.33	2.14	5.49	22.39
0.43	2.45	2.44	25.71
0.55	2.82	1.05	29.52
0.69	3.23	0.42	33.90
0.98	3.71	0.16	38.93
1.49	4.26	0.06	44.70
2.04	4.89	0.02	51.32
3.08	5.62	0.01	58.93

Numerical Method

The commercial software package FLUENT (version 6.2.16) from Ansys, Inc. is adopted for this study. The simulation uses the segregated solver, which employs an implicit pressure-correction scheme and decouples the momentum and energy equations according to the FLUENT manual [23]. The SIMPLE algorithm is used to couple the pressure and velocity. The second order upwind scheme is selected for spatial discretization of the convective terms and species. Lagrangian trajectory calculations are employed to model the dispersed phase of droplets. The impact of droplets on the continuous phase is considered as a source term in each of the governing equations. After obtaining an approximate flow field of the continuous phase (airflow in this study), droplets are injected, and their trajectories are calculated. At the same time, drag and heat and mass transfer between the droplets and the airflow are calculated.

Iterations proceed alternatively between the continuous and discrete phases. Twenty iterations in the continuous

phase are conducted between two consecutive iterations in the discrete phase. Converged results were obtained after the specified residuals are met. A converged result renders a mass residual of 10^{-3} , an energy residual of 10^{-6} , and momentum and turbulence kinetic energy residuals of 10^{-3} . These residuals are the summation of the imbalance for each cell and are scaled by a representative of the flow rate. Typically, 400 to 500 iterations are needed to obtain a converged result in each time step.

Comparison of Different Turbulence Models and Stochastic Time Constants

Comparisons have been made between different turbulence models for the staggered silencer geometry with the fogging system installed upstream of the silencer with wet wall boundary conditions. (Case 5, to be described later) The temperature drop and the amount of water evaporated are chosen as the comparing parameters. The result shows that the temperature drop for all turbulence models is in the range between 16 and 16.5°C except the k- ω standard model which results in a temperature drop of 12.1°C, as shown in Table 2. The amount of water evaporated is approximately proportional to the drop of temperature; i.e. a higher evaporation rate accompanied by a larger temperature drop, except in the k- ω standard model.

According to Wang and Dhanasekaran [11], the time constant (C_t) used in scaling the turbulence eddy size in the stochastic tracking method may significantly affect the results of particle tracking in certain flow conditions, so a sensitivity study is conducted to inspect its influence on the CFD results of this paper. Four different time constants, ranging from 0.15 to 0.0001, are used. Table 3 shows that the temperature drop is within 0.32°C and is not so sensitive among the first three larger C_t values in this study. The value of 0.15 is used for all cases.

Table 2 Comparison among different turbulence models (Based on Case 5)

Models	Parameters					
	Inlet Static Temp. (K)	Exit Static Temp. (K)	Temp. Drop (K)	Inlet Flow Rate (kg/s)	Exit Flow Rate (kg/s)	Evap. Water (kg/s)
k- ϵ Standard	323.00	306.50	16.50	82.892	83.536	0.644
k- ϵ RNG	323.00	306.89	16.11	82.892	83.520	0.628
k- ϵ Realizable	323.00	306.76	16.24	82.892	83.539	0.647
k- ω Standard	323.00	310.90	12.10	82.892	83.571	0.665
k- ω SST	323.00	306.34	16.66	82.892	83.552	0.660

Table 3 Comparison among different time constants used in stochastic particle tracking scheme (Base on Case 5)

Models	Parameters					
	Inlet Static Temp. (K)	Exit Static Temp. (K)	Temp. Drop (K)	Inlet Flow Rate (kg/s)	Exit Flow Rate (kg/s)	Evap. Water (kg/s)
$C_t = 0.15$	323.00	306.50	16.50	82.892	83.536	0.644
$C_t = 0.01$	323.00	306.57	16.43	82.892	83.535	0.643
$C_t = 0.001$	323.00	306.82	16.18	82.892	83.517	0.626
$C_t = 0.0001$	323.00	307.49	15.51	82.892	83.491	0.599

Comparison of Different Mesh Numbers

A grid sensitivity study also based on Case 5 is made with two different numbers of cells, 121,000 and 231,000, respectively. In the finer grid, the mesh size has almost doubled, which gives almost 24% excess nodes than the smaller one in 3 dimensions. Results are shown in Table 4. The temperature drop and the amount of water evaporated are found to be within 1.54% and 3.04%, respectively. Since the change is not large, all the cases presented in this study use the finer grid of 231,000 cells. A further refinement of the grid size is not pursued in this study.

Table 4 Comparison among different mesh numbers

Number of meshes	Parameters							
	Inlet Static Temp. (K)	Exit Static Temp. (K)	Temp. Drop (K)	Diff. from 121K mesh	Inlet Flow Rate (kg/s)	Exit Flow Rate (kg/s)	Evap. Water (kg/s)	Diff. from 121K mesh
121K	323.00	306.75	16.25	N.A.	82.892	83.517	0.625	N.A.
231K	323.00	306.50	16.50	1.54%	82.892	83.536	0.644	3.04%

RESULTS AND DISCUSSION

Studied Cases

- Case 1: Single silencer, water sprayed upstream of the silencer, droplets are reflected from wall.
- Case 2: Single silencer, water sprayed upstream of the silencer, droplets wet the wall surface.
- Case 3: Single silencer, water sprayed downstream of the silencer.
- Case 4: Staggered silencer, water sprayed upstream of the silencer, droplets are reflected from wall.
- Case 5: Staggered silencer, water sprayed upstream of the silencer, droplets wet the wall surface.
- Case 6: Staggered silencer, water sprayed downstream of the silencer.

The term "single silencer" means the silencer is made with one single row of baffles and "staggered silencer" means the silencer is made with two rows of staggered baffles. As mentioned earlier, the water is sprayed in two different locations: the first one is located at the inlet of the silencer sub-domain, upstream of the silencer, represented by Cases 1, 2, 4 and 5); the second one is located right downstream of the silencer, represented by Cases 3 and 6. The boundary condition for droplets at the walls can be assigned as reflected, trapped, or maintaining as a liquid film, as mentioned earlier. Since all three conditions could occur in the real application but Fluent code only allows one condition to be assigned at a time, this study employs both reflected and wall-film boundary conditions at separated cases. Two different boundary conditions have been assumed for the discrete phase, as mentioned earlier: (a) reflected condition – water droplets bounce back elastically from the surface once they reach the silencer wall (Cases 1, 3, 4 and 6) and (b) wall-film condition; water droplets stick to the wall and wet the surface when they reach any of the walls in the domain (Cases 2 and 5).

Temperature Distribution

When the fogging is applied, the hot and dry air gets cooler and moistened as it passes along the inlet duct. Figure 7 shows the cross-sectional temperature distributions of all six cases at selected locations along the duct and Fig. 8 shows the temperature distributions on the longitudinal mid-plane along the duct.

Effect of discrete phase wall boundary conditions (Case 1 vs. Case 2 and Case 4 vs. Case 5) -- Cases 1 and 2 show very close temperature distributions, so they are shown in one figure and the same is true for Cases 4 and 5. This implies that the two different wall boundary conditions for droplets, either reflected or wall-filmed, have negligible effects on the calculated results under the current droplet-wall interaction models and studied conditions.

Effect of upstream vs. downstream fogging (Cases 1&2 vs. Case 3 for single silencer and Cases 4&5 vs. Case 6) -- When the fogging system is moved from upstream to downstream of the silencer, the distance the droplets have to travel to reach the GT inlet is reduced approximately 4.3 m with a reduction of residence time approximately of half second. So Case 3 shows less temperature reduction through the duct in Fig. 7b. Table 5 shows that the shortened distance translates to about 0.5°C less temperature drop, as exit temperature for Case 3 being 307.16K versus 306.65K and 306.66K for Cases 1 and 2, respectively. The difference does not seem to be large to cause any concern. The same result of about a 0.5°C difference in exit temperature is true for Cases 4&5 vs. Case 6 with the staggered silencer (see Table 5). This fact is further supported by the percentage of water evaporated, as shown in Table 5. Percentage of water evaporated for the Cases 1&2 is 92.5% vs 86.8% for Case 3, while this value for Cases 4&5 is more than 94% vs 87% for Case 6. Comparing cross-sectional temperature distribution at the inlet of compressor (or exit of inlet duct) in Figs. 8(a) vs. 8(b) and 8(c) vs. 8(d), it looks that the temperature is more uniformly distributed in cases of locating the fogging upstream of the silencer. A more uniformly distributed temperature also has the benefit of reducing thermal stresses on the compressor blades.

Effects of a single row of baffles vs. staggered baffles (Group 1: Cases 1&2 vs. Cases 4&5 and Group 2: Case 3 vs. Case 6) - The effects of a single silencer versus a staggered silencer can be categorized into two groups of comparisons. The first group comparison is Cases 1&2 versus Cases 4&5, which include both the influences of fluid mechanics and the droplet wall boundary conditions; whereas the second group comparison between Cases 3 and 6 only shows the influence of fluid mechanics because the fogging system is installed downstream of the silencer in both cases.

(a) Group 1 comparison: Cases 4 and 5 have staggered baffles, which impose more obstruction for the droplets and, hence, have more turbulent mixing for droplet evaporation than in the single silencer cases. The exit temperatures for Cases 4&5 do show about a 0.15°C greater temperature drop than Cases 1&2 with the single silencer (Table 5). Again, this minor difference in temperature drop (0.15°C) does not warrant much interpretation of the difference between a single silencer and staggered silencers.

(b) Group 2 comparison: It is interesting to see that the comparison between Case 3 and Case 6 also reaches the same result as Group1 with a minor 0.15°C temperature drop

difference, even though the fogging system is installed downstream of the silencer in both cases and droplets do not encounter the baffles in the silencer. This implies that the influence of the flow fields induced by the different configurations of the baffles is more responsible for droplet evaporation even downstream of the silencer.

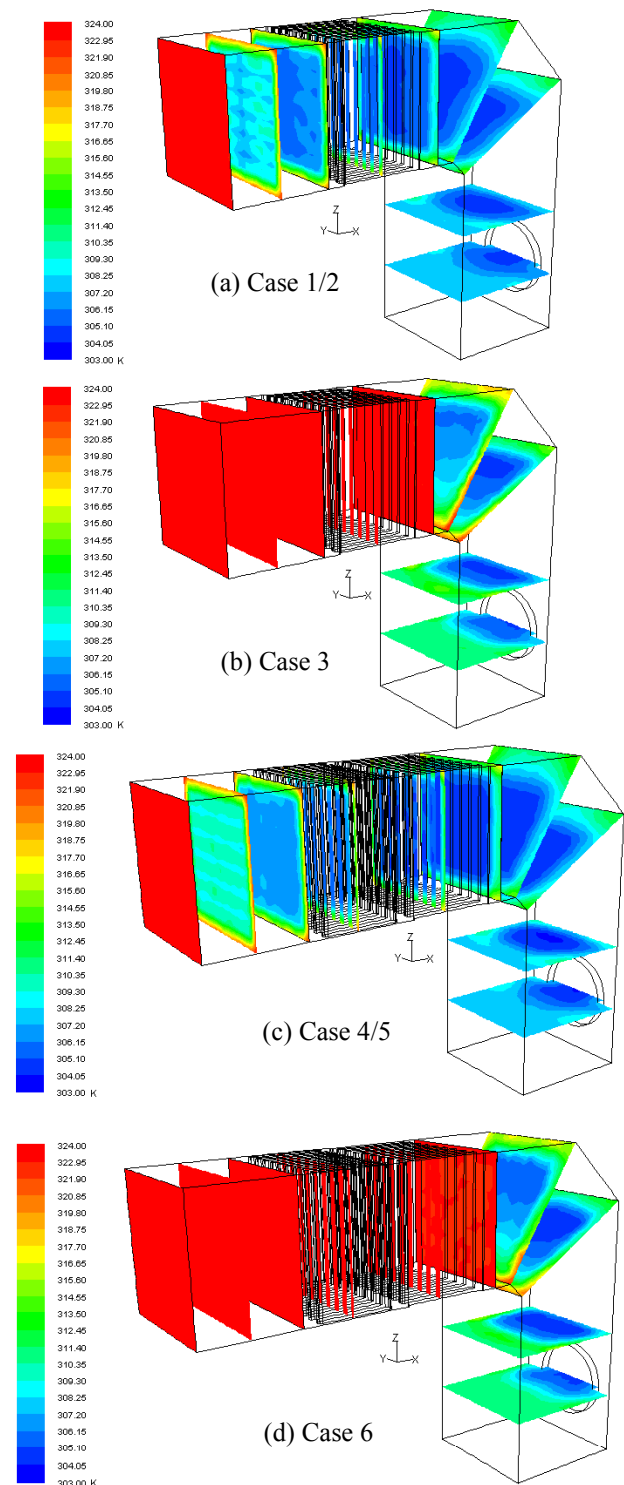


Figure 7 Temperature distributions for different cases on different axial planes

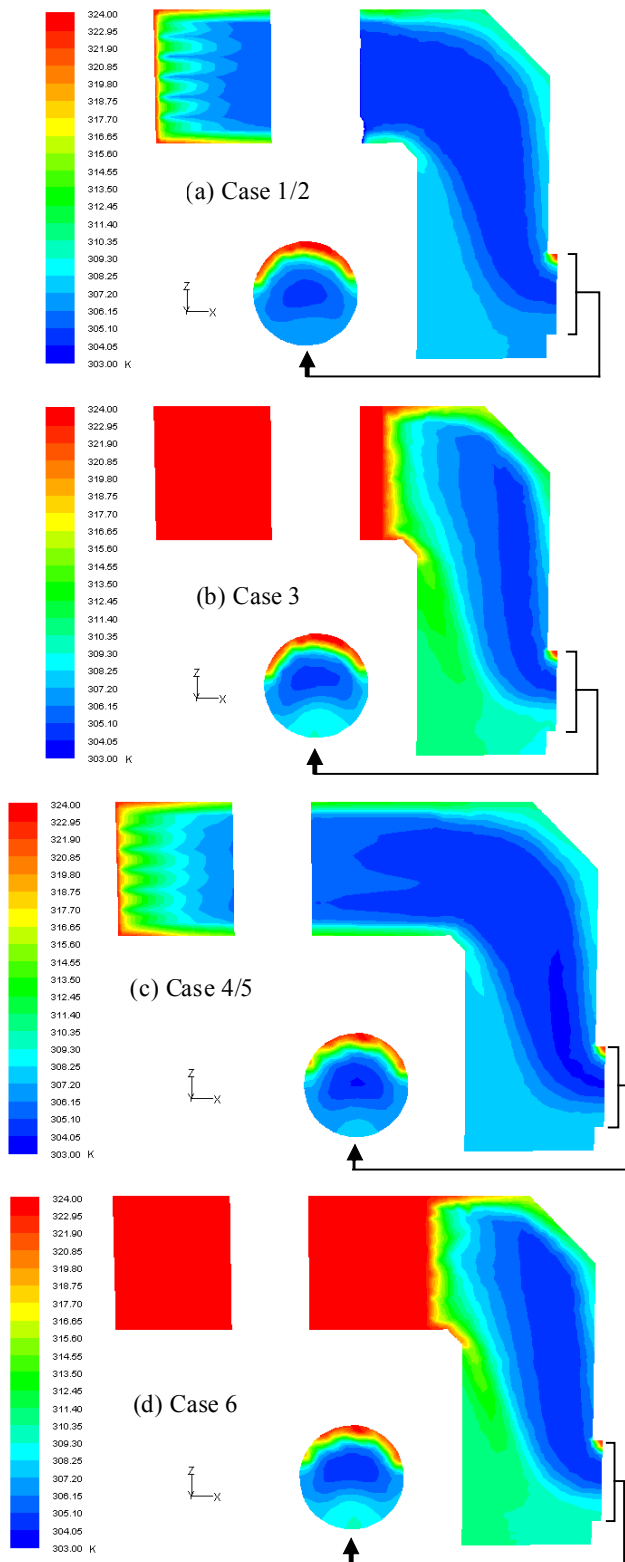


Figure 8 Temperature distributions for different cases on the longitudinal mid-plane along the duct. (The gaps are due to the plane cutting through a silencer baffle which is not included in the computational domain. The circles in each figure shows the cross-sectional temperature distribution at the compressor bell-mouth inlet.)

Figure 7 shows that the lower temperature region moves towards the wall adjacent to the exit for all the cases, as the flow is subjected to secondary flow activities when it passes

through the bend. Figure 8 shows the temperature distribution on the longitudinal mid-plane along the duct axis. The effect of staggered baffles on temperature can be seen between Fig. 8a and 8c. Figure 8a shows a very non-uniform temperature field with sharp lateral temperature gradients, which is in contrast to a relatively more uniform temperature gradient shown in Fig. 8c, presumably due to the more turbulent mixing introduced by the staggered two rows of baffles than the single row of baffles. Figure 8b and 8d show the temperature distributions for downstream spray. These two figures show almost identical distributions, as the distance from the spraying nozzle to the bellmouth is same for both the cases and the effect of silencer is minimal.

In addition to higher turbulent mixing in cases 5 & 6 which enhance the evaporation efficiency, the improvement in efficiency is due to the fact that the droplets residence time is higher in the case of staggered silencer with longer subdomain (4.3 m) when compared to the one for single silencer subdomain (2.6 m). All other duct dimensions are the same.

Table 5 Comparison among different cases

Cases	Temp. Drop (K)	T_{ex} from CFD (K)	Sp. Hum. at Exit (kg/kg DA)	Exit Vel. (m/s)	Evap. Water (kg/s)	% of Water Evap.	Liq. water at silencer (kg)	Evap. Eff. (%)	Press drop (Pa)
Case 1	16.35	306.65	0.0284	41.46	0.631	92.52	0.0202	91.85	1517
Case 2	16.34	306.66	0.0281	41.38	0.631	92.52	0.0252	91.80	1515
Case 3	15.84	307.16	0.0280	41.40	0.592	86.80	N.A.	88.99	1525
Case 4	16.49	306.51	0.0259	39.98	0.643	94.28	0.0306	92.64	1615
Case 5	16.50	306.50	0.0259	39.98	0.644	94.43	0.0305	92.70	1615
Case 6	15.97	307.03	0.0280	40.12	0.593	86.95	N.A.	89.72	1629

Flow Field

The flow field is shown in the velocity vector plots in Fig. 9. A large recirculation is found near the compressor bell-mouth's inlet. An increase in velocity is found in the second stage of the staggered silencer case (Fig. 9b). The initial velocity is 10m/s, which increases to 25m/s at the end of the staggered silencer. The mass weighted average velocity at the exit is 41.4m/s for the single silencer and 40m/s for the staggered silencer, as shown in Table 5. This difference of average velocity is caused by density difference directly related to the difference in cooled air temperatures between the two cases to keep the constant mass flow rate, as it is mentioned in the boundary condition.

A close-up view of the airflow pathlines surrounding the silencer's staggered baffles is shown in Fig. 10. A stagnation region can be seen at the nose of the baffle. A closed separation wake is found at the trailing edge of the baffle (Fig. 10). The static pressure distribution is shown in Fig. 11. High static pressure (in red) is shown near the stagnation region in front of the silencer baffles. High velocity and low pressure are seen in the passage between the two baffles, and some static pressure is recovered downstream of the baffles (in yellow). The pressure drop for the single silencer (Case 1) is 1517 Pa (6 inch H₂O or 0.22 psi) vs. 1615 Pa (6.5 inch H₂O or 0.234 psi) for the staggered silencer (Case 4). The difference is about 6.5%.

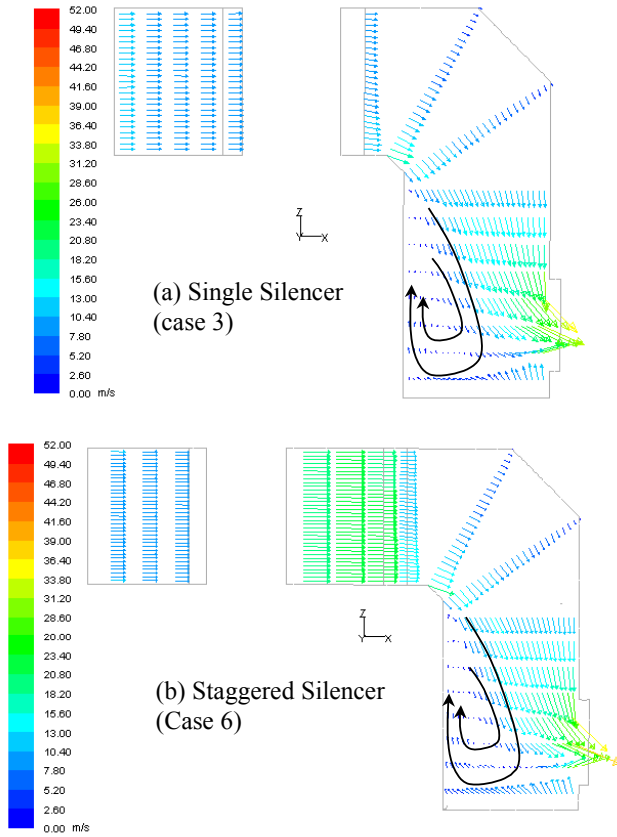


Figure 9 Velocity vectors for different silencers (Circulation is shown by arrows)

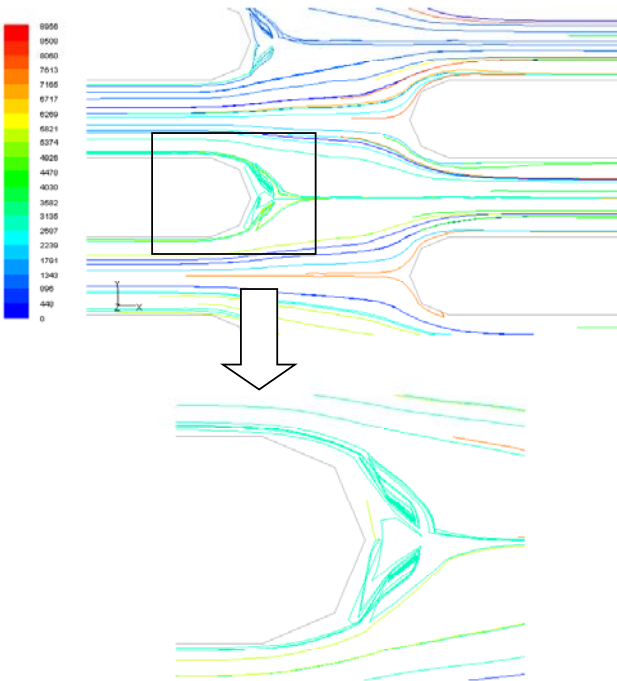


Figure 10 Air pathlines surrounding the silencer's staggered baffles

Discrete Phase Results

The droplets are so small that they flow with the main fluid very easily. Figure 12 shows the droplet traces colored by the droplet Reynolds number surrounding the silencer baffles.

The droplet Reynolds number is calculated based on the slip velocity between the droplet and the air speed in the continuous phase. Comparing the droplet traces in Fig. 12 and the airflow pathlines in Fig. 9, the wiggling droplet traces illustrate the effect of stochastic tracking scheme imposed on the droplets. The typical droplet Reynolds number is around 10 near the spraying location. The droplets usually quickly reach equilibrium in force balance and the droplet Reynolds number is typically reduced to less than 0.5. In the bend section, the droplet Reynolds number may change again due to the centrifugal force. This fact can be observed from Fig. 12. Droplets get scattered as soon as they encounter the silencer baffles' tips. Some Reynolds numbers close to 10 are found in between the two silencers. The Reynolds number stays close to 10^{-7} in the rest of the duct, when the local body forces such as acceleration, deceleration, and centrifugal forces are absent. Figure 12 shows no significant difference for different droplet wall boundary conditions. Although the model in Fig 12(a) has the reflect boundary condition for droplet, but only limited discernable reflections are observed.

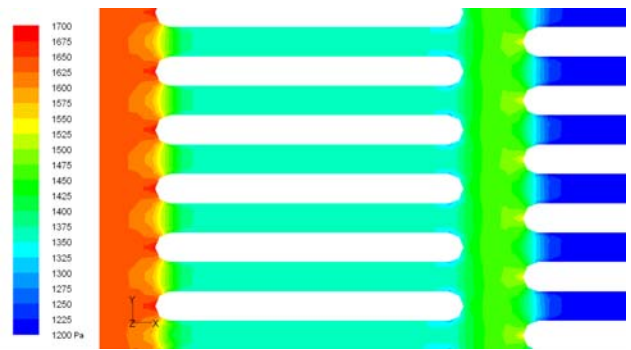


Figure 11 Static pressure distribution across the baffles

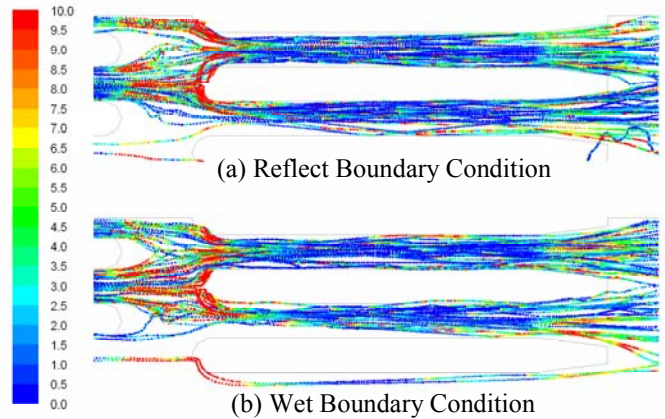


Figure 12 Droplet traces colored by the droplet Reynolds Number surrounding the silencer baffles.

Figure 13 shows the discrete phase model (DPM) concentration distributions at the mid horizontal plane for cases with fogging applied upstream of both types of silencers. Most of the droplets evaporate before the bend. Different droplet wall boundary conditions (reflected vs. wall-film) show negligible effects on the droplet

concentration distribution. The amount of liquid water found in the silencer subdomain is 0.0202kg for the single silencer and 0.0252kg for the staggered silencer with a reflect type boundary condition

The mass-weighted average exit temperature has been used as a criterion to evaluate the fogging performance in all above analyses, but the comparison of the exit temperatures doesn't provide the information on what has been achieved relatively to different inlet conditions (eg. different ambient temperature and RH values). The evaporation effectiveness defined in Eq. 21 can then provide such a gauge:

$$E = \frac{DBT - T_{Ex}}{DBT - WBT} \quad (21)$$

From the values in Table 5, it can be seen that installing the fogging upstream of the silencer is about 3 percentage points better in evaporation effectiveness than placing it downstream of the silencer, irrespective of whether the silencer consists of a single row of baffles or two rows of staggered baffles, as water gets more residence time for evaporation in cases of upstream spray. The evaporation effectiveness of the staggered silencer is about 0.8 percentage points higher than the single silencer.

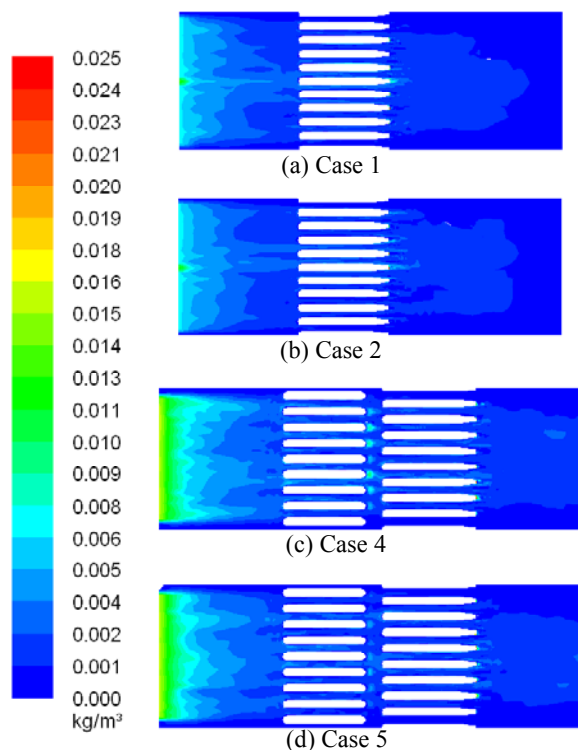


Figure 13 DPM concentration for mid-horizontal plane for the cases where fogging is applied upstream of the silencer

CONCLUSIONS

CFD simulations have been performed to investigate the fogging performance regarding placing the fogging system upstream versus downstream of the silencer with two different silencers consisting of one single row of baffles versus two rows of staggered baffles. The summary of these findings is:

- The effect of using two different types of droplet wall boundary conditions (reflect vs, wall-film) on the calculated evaporation rate is negligible.
- Keeping the fogging system upstream and downstream of the silencer shows almost negligible (3% more for upstream) difference in temperature drop, irrespective of single or staggered arrangement.
- Temperature distribution is more uniform in cases of locating the fogging before the silencer. This has the beneficial effect of reducing thermal stresses on the compressor blades.
- Installing the fogging system upstream of the silencer is about 3 percentage points better in evaporation effectiveness than placing it downstream of the silencer, irrespective of whether the silencer consists of a single row of baffles or two rows of staggered baffles.
- The evaporation effectiveness of the staggered silencer is about 0.8 percentage points higher than the single silencer.
- The pressure drop for the staggered silencer is about 6.5% higher than the single silencer.

ACKNOWLEDGMENTS

This study was supported by the Louisiana Governor's Energy Initiative via the Clean Power and Energy Research Consortium (CPERC) and administered by the Louisiana Board of Regents.

REFERENCES

1. Cortes, C.R. and Willems, D.E., 2003, "Gas Turbine Inlet Air Cooling Techniques: An Overview of Current Technologies," POWER-GEN, Las Vegas, Neva, USA.
2. Angello, L., 2005, "Axial Compressor Performance Maintenance Guide Update," EPRI Technical Update, Document# 1008325.
3. Acoustical Surfaces Inc., "Silent-Mod Duct Silencer", 2010, <http://www.acousticalsurfaces.com>.
4. American Air Filter, "Rectangular Duct Mute", 2010, <http://www.aafintl.com>.
5. UNCER Technologies Inc., "UNCER Silencer", 2010, <http://www.enoisecontrol.com>.
6. Industrial Acoustics Company, "IAC Silencer", 2010, <http://www.soundcontrol4less.com>.
7. Chaker, M., Meher-Homji, C.B. and Mee, T.R., 2004, "Inlet Fogging of Gas Turbine Engines—Part I: Fog Droplet Thermodynamics, Heat Transfer, and Practical Considerations," *Journal of Engineering for Gas Turbines and Power*, July 2004, Vol. 126, pp. 545-558.
8. Chaker, M., Meher-Homji, C.B., and Mee, T.R., 2004, "Inlet Fogging of Gas Turbine Engines—Part II: Fog Droplet Sizing Analysis, Nozzle Types, Measurement, and Testing," *Journal of Engineering for Gas Turbines and Power*, July 2004, Vol. 126, pp. 559-570.
9. Chaker, M., Meher-Homji, C.B., and Mee, T.R., 2004, "Inlet Fogging of Gas Turbine Engines—Part III: Fog

- Behavior in Inlet Ducts, Computational Fluid Dynamics Analysis, and Wind Tunnel Experiments," *Journal of Engineering for Gas Turbines and Power*, July 2004, Vol. 126, pp. 571-580.
10. Li, X., and Wang, T., 2007, "Effects of Various Modelings on Mist Film Cooling," *ASME Journal of Heat Transfer*, vol. 129, pp. 472-482.
 11. Wang, T. and Dhanasekaran, T.S., 2010, "Calibration of CFD Model for Mist/Steam Impinging Jets Cooling," *ASME Journal of Heat Transfer*, Vol. 132, Issue 12, 122201/1-11, 2010
 12. Wang, S., Liu, G., Mao, J., and Feng, Z., 2007, "Experimental Investigation on the Solid Particle Erosion in the Control Stage Nozzles of Steam Turbine," *Proceedings of ASME Turbo Expo 2007*, Montreal, Canada, May 14-17, 2007, ASME Paper: GT2007-27700.
 13. Schiller, L., and Naumann, A., 1933, "Uber die grundlegenden Berechnungen bei der Schwekraftaubereitung," *Zeitschrift des Vereines Deutscher Ingenieure*, 77(12), 318-320.
 14. Ranz, W. E. and Marshall, W. R. Jr., 1952, "Evaporation from Drops, Part I," *Chem. Eng. Prog.*, 48, pp. 141-146.
 15. Ranz, W. E. and Marshall, W. R. Jr., 1952, "Evaporation from Drops, Part II," *Chem. Eng. Prog.*, 48, pp. 173-180.
 16. Kuo, K. Y., 1986, *Principles of Combustion*, John Wiley and Sons, New York.
 17. Watchers, L. H. J., and Westerling, N. A., 1966, "The Heat Transfer from a Hot Wall to Impinging Water Drops in the Spheroidal State", *Chem. Eng. Sci.*, Vol.21, pp. 1047-1056.
 18. Harlow, F. H., and Shannon, J. P., 1967, "The Splash of a Liquid Drop", *Journal of Applied Physics*, No. 38, pp. 3855-3866.
 19. Bai, C., and Gosman, A. D., 1995, "Development of Methodology for Spray Impingement Simulation," SAE Paper No. 950283.
 20. Stanton, D. W., and Rutland, C. j., 1996, "Modeling Fuel Film Formation and Wall Interaction in Diesel Engines," SAE Paper No. 960628.
 21. Rourke, P. J. O., and Amsden, A. A., 2000, "A Spray/Wall Interaction Submodel for the KIVA-3 Wall Film Model," SAE Paper No. 2000-01-0271.
 22. Dhanasekaran, T. S. and Wang, T., " Model Verification of Mist/Steam Cooling with Jet Impingement Onto a Concave Surface and Prediction at Elevated Operating Condition," ASME Paper No. GT2010-22238, *Proceedings of ASME Turbo Expo2010*, Glasgow, UK, June 14-18, 2010
 23. *Fluent Manual*, Version 6.3, 2008, Fluent, Inc.